ADVANCED MATERIALS

Supporting Information

for *Adv. Mater.*, DOI: 10.1002/adma.201906806

Hydration-Effect-Promoting Ni–Fe Oxyhydroxide Catalysts for Neutral Water Oxidation

Ning Wang, Zhen Cao, Xueli Zheng, Bo Zhang, Sergey M. Kozlov, Peining Chen, Chengqin Zou, Xiangbin Kong, Yunzhou Wen, Min Liu, Yansong Zhou, Cao Thang Dinh, Lirong Zheng, Huisheng Peng, Ying Zhao, Luigi Cavallo, Xiaodan Zhang,* and Edward H. Sargent**

Supplementary Information for

Hydration-Effect-Promoting Ni-Fe Oxyhydroxide Catalysts for Neutral Water Oxidation

Ning Wang, Zhen Cao, Xueli Zheng, Bo Zhang, Sergey M. Kozlov, Peining Chen, Chengqin Zou, Xiangbin Kong, Yunzhou Wen, Min Liu, Yansong Zhou, Cao Thang Dinh, Lirong Zheng, Huisheng Peng, Ying Zhao, Luigi Cavallo, Xiaodan Zhang and Edward H. Sargent

Materials and Methods

Chemicals. Iron (III) chloride ($FeCl_3$), nickel (II) chloride hexahygrate ($NiCl_6 \cdot 6H_2O$), magnesium chloride hexahydrate ($MgCl_2 \cdot 6H_2O$), calcium chloride ($CaCl_2$), strontium chloride hexahydrate ($SrCl_2 \cdot 6H_2O$), barium chloride dehydrate ($BaCl_2 \cdot 2H_2O$), ethanol (≥99.5%), propylene oxide (≥99%) and nafion solution (5wt%) were purchased from Sigma-Aldrich. All chemicals were used without further purification.

Synthesis of gelled Ni-Fe-Mg catalysts. Gelled Ni-Fe-Mg catalysts were synthesized using a modified aqueous sol-gel technique. $NiCl_6 \cdot 6H_2O$ (2.1 mmol), anhydrous $FeCl_3$ (0.35 mmol) and $MgCl_2 \cdot 6H_2O$ were first dissolved in ethanol (2mL) in a vial. A solution of deionized water (DI) (0.18 mL) in ethanol (2 mL) was prepared in a separate vial. All solutions mentioned above were cooled in an ice bath for 2 hours to prevent uncontrolled hydrolysis and consideration which may lead to the formation of precipitate rather gel formation. The Ni, Mg and Fe precursors were then mixed with

an ethanol-water mixture to form a clear solution. Propylene oxide (≈ 1 mL) was then slowly added to form a gel. Finally, the prepared Ni-Fe-Mg wet-gel was aged for 24 hours to promote network formation and immersed in acetone for 5 days before the gel was vacuum drying.

Gelled Ni-Fe-Ca, Ni-Fe-Sr and Ni-Fe-Ba were synthesized following a similar process to that of Ni-Fe-Mg except with the addition of $CaCl_2$, $SrCl_2 \cdot 6H_2O$ and $BaCl_2 \cdot 2H_2O$ as precursors.

Characterization. A FEI scanning electron microscopy (SEM) images and energy-dispersive X-ray spectroscopy mapping operated at 1.5 kV were used to characterize the surfaces of all samples. Transmission electron microscopy (TEM) and electron energy loss spectroscopy (EELS) elemental maps were taken on a Philips, FEI CM12 instrument. The samples were prepared by a drop-casting method onto carbon-coated copper TEM grids. X-ray diffraction (XRD) data were collected in Bragg Brentano mode using 0.02° divergence with a scan rate of 0.1 °/s. Nitrogen BET surface area measurements were performed to determine the specific surface areas of the catalysts. N_2 adsorption-desorption isotherms of the catalysts were measured at -196 °C using a TriStar II Plus. The samples were outgassed under vacuum for 10 h at 100 °C prior to the measurements. Water molecule adsorption measurements were investigated using X-ray photoelectron spectroscopy (XPS, Thermo WSCALAB 250) and Fourier transform infrared (FTIR) spectroscopy (Thermo Nicolet 6700).

***In situ and quasi in situ* X-ray absorption.** We acquired Ni and Fe K-edge X-ray absorption near-edge structure spectroscopy (XANES) and Fourier-transformed extended X-ray absorption fine structure (FT-EXAFS) data to assess electronic structure of Ni. These were collected at the 1W1B beamline at the Beijing Synchrotron Radiation Facility. The scanning energy range of Ni K-edge and Fe K-edge were set from 8.320 keV to 8.420 keV and 7.100 keV to 7.200 keV, respectively, in fluorescence mode. The pre-edge of Ni XANES in Ni-Fe-Mg catalyst after oxidizing reaction were shifted to higher energy compared with Ni_2O_3 and NiO. This indicates that the oxidation state of Ni in Ni-Fe-Mg at 2.2 V vs. RHE is higher than that of Ni^{3+}.

Simulations of EXAFS spectra were carried out using the FEFF8.5 codes embedded in the *Artemis* software. The crystallographic information file (CIF) of $Ni(OH)_2$ was used in the calculation of raw scattering paths. The experimental spectra were fitted with the aid of raw scattering paths at a K-range of 3 to 13 $Å^{-1}$.

FTIR spectroscopy. All the IR spectra were recorded on a FTIR spectrometer at a resolution of 2/cm and 32 scans for each spectrum. The sample-KBr pellets were weighed (2 mg sample ground with 100 mg KBr) and pressed under a load of 10 MPa in a 13 mm die. The IR spectra were recorded at ambient temperature of 23 - 25℃ and 25 - 35% relative humidity. In order to investigate water adsorption using the FTIR, we normalize the FTIR transmittance (specific transmittance) using equation below:

$$Specific\ transmittance = \frac{FTIR\ Transmittance}{Mass \times Area_{BET}} \qquad (1)$$

where FTIR specific transmittance is obtained from FTIR spectrometer, *Mass* is the

catalyst mass and $Area_{BET}$ is specific surface area obtained from the Brunauer-Emmett-Teller (BET) method.

Electrochemical characterization. Electrochemical measurements were performed using a three-electrode system connected to an electrochemical workstation (Autolab PGSTAT302N) with built-in electrochemical impedance spectroscopy (EIS) analyzer. The working electrode was a glass carbon electrode (GCE) (diameter: 3 mm, area: 0.072 cm^2) from CH Instruments. GCEs were polished with two different alpha alumina powders (1.0 and 0.3 μm from CH Instruments) suspended in deionized water on a Nylon polishing pad (CH Instruments). After the first and second stages of cleaning, the electrodes were thoroughly rinsed with deionized water. Before loading catalysts, the electrodes were also cleaned by immersing them in an isopropanol solution with sonication for 10 seconds. Ag/AgCl (with saturated KCl as the filling solution) and platinum foil were used as reference and counter electrodes, respectively.

Typically, 4 mg of catalyst powder was dispersed in a 1 ml mixture of water and ethanol (4:1, v/v), and then 80 μl of Nafion solution (5 wt.% in water) was added. The suspension was immersed in an ultrasonic bath for 30 min to prepare a homogeneous ink. The working electrode was prepared by dipping 5 μl catalyst ink onto GCE (catalyst loading 0.21 mg/cm^2).

To load the catalyst on the Ni foam (thickness: 1.6 mm, Sigma), 20 mg of catalyst was dispersed in a mixture containing 2 ml of water and 2 ml ethanol, followed by the addition of 100 μl Nafion solution. The suspension was sonicated for 30 min to prepare

a homogeneous ink. Ni foam with a fixed area of 0.5 × 0.5 cm^2 coated with water resistant silicone glue drop-casted with 20 μl of the catalyst ink.

Cyclic voltammetry (CV) measurements at 50 mV/s were performed prior to recording linear scan voltammetry (LSV) at 1 mV/s for each sample. EIS measurements were conducted in static solution at 1.6 V (vs. RHE). The amplitude of the sinusoidal wave was 10 mV, and the frequency scan range was from 100 kHz to 0.01 Hz. Unless otherwise stated, all experiments were performed at ambient temperature (23±2 ℃) and electrode potential was converted to the RHE scale using

$$E(vs.RHE) = E(vs.Ag/AgCl) + E_{Ag/AgCl}(vs.NHE) + 0.059 \times pH \quad (2)$$

The kinetics of OER are increased at elevated temperatures, reflecting the temperature dependence of the chemical rate constant, which is approximately proportional to exp(-$\Delta H^*/kT$), where ΔH^* is the apparent enthalpy of activation (hereafter simply termed as the activation energy), and k is the Boltzmann constant. In particular, the apparent electrochemical activation energy (E_a) for water oxidation can be evaluated at a fixed overpotential (η = 600 mV) using the Arrhenius relationship below,

$$\frac{\partial(log i_k)}{\partial(1/T)}|_\eta = \frac{\Delta H^*}{2.3R} \quad (3)$$

using a temperature range between 21℃ and 41℃. The Arrhenius plots for fixed overpotential for three different catalysts are shown Figure 2d, all of which reveal a linear dependence on inverse temperatures. From the slope of the Arrhenius plot, the E_a of three catalysts is obtained.

Turnover frequency (TOF) determination. The number of active sites is calculated using the following equation:

$$n_{Ni} = \frac{Q_{Ni}}{F} \times NA \quad (4)$$

where Q_{Ni} is the integration area of Ni redox peak from CV curves, F is the Faraday constant, NA is Avogadro's constant, assuming that Ni^{2+}/Ni^{4+} is a two-electron process. The TOF value was calculated from equation:

$$TOF = \frac{J \times A \times \eta}{4 \times F \times n} \quad (5)$$

J is obtained at 1.73 V vs. RHE, normalized by geometric area, A is the geometric area, F is the Faraday constant and η is the Faradaic efficiency. n is the mole number of active atoms on the electrode, calculated from equation (3) above.

Electrochemical active surface area (ECSA). The electrochemically active surface area of each catalyst on different supports was obtained based on measurement of their electrochemical capacitances. We measured the CVs in a narrow non-Faradaic potential window in which the change of the current is principally due to the charging of the double-layer, which is expected to be linearly proportional to the active surface area. The measured capacitive current densities at the average potential in the selected range were plotted as a function of scan rates and the slope of the linear fit was calculated as the double-layer capacitance (C_{dl}). The specific capacitance was found to be 40 μF/cm^2. The ECSA of the catalyst is calculated from the following equation,

$$ECSA = \frac{C_{dl}}{40\mu F/cm^2} cm^2_{ECSA} \quad (6)$$

The intrinsic activity was obtained by normalizing the current to the ECSA to exclude

the effect of surface area on catalytic performance.

IR correction. All the polarization curves on different supports in this work were corrected for ohmic losses (including the wiring, substrate, catalyst and solution resistances). The iR-corrected data is given by the equation:

$$E_{Corrected} = E - iR \qquad (7)$$

where R is the series resistance of measurement, which can be obtained from an EIS Nyquist plot as the first intercept of the main arc with the axis.

Density functional theory molecular dynamics (DFT-MD) simulation setup. Two representative test systems, namely, the Ni-Fe-Mg and Ni-Fe-Ba catalysts, were selected to explore the water adsorption on the catalysts surface. The models were constructed based on the β-NiOOH.[1] The surface hydrogen atoms were described based on the Pourbaix diagrams.[2] To emphasize the trend of surface hydration, we replace four surface Ni atoms by Mg atoms or Ba atoms, which are higher than the synthesized catalyst. The catalyst was first optimized at the PBE level [3] of density functional theory (DFT) using the VASP package. [4] The electrons were described using the Projector Augmented-Wave (PAW) method [5] with a 450 eV energy cutoff. The van der Waals (vdW) interactions were described using the Grimme's correction. [6] The DFT-MD simulations were performed in canonical ensemble at 300 K using the Nose-Hoover thermostat. [7] We performed the simulation for 12 ps, and the last 10 ps trajectory was recorded for the analysis.

Single ion-water pair structure optimization. The distance between the M^{2+} cation and water molecule obtained from the PBE level of DFT calculation implemented in the Gaussian09 package.[8] The electrons were described using the hybrid basis sets: aug-cc-pvtz[9] for non-metal atoms and LANL2DZ[10] for metal atoms. The vdW interactions were described using the Grimme's correction.

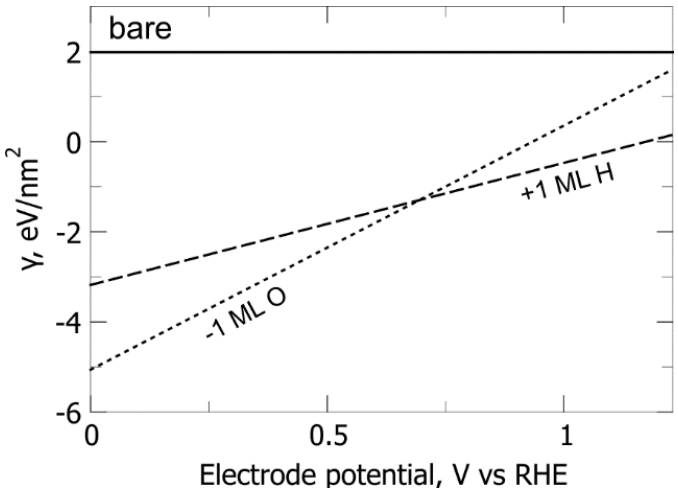

Figure S1 Surface energy of various surface terminations for NiOOH ($0\bar{1}5$) surface. The surface termination with the lowest γ prevails at a given electrode potential.

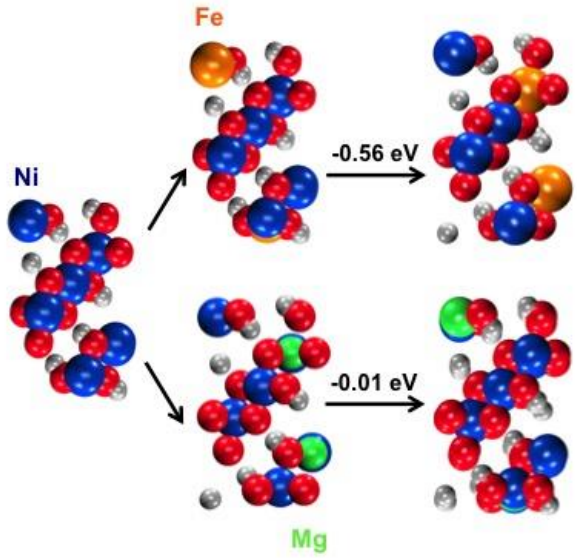

Figure S2 Relative energy of doping Fe/Mg to the different positions of NiOOH slab: the Fe prefers the subsurface positions, while the Mg does not have preferred doping positions.

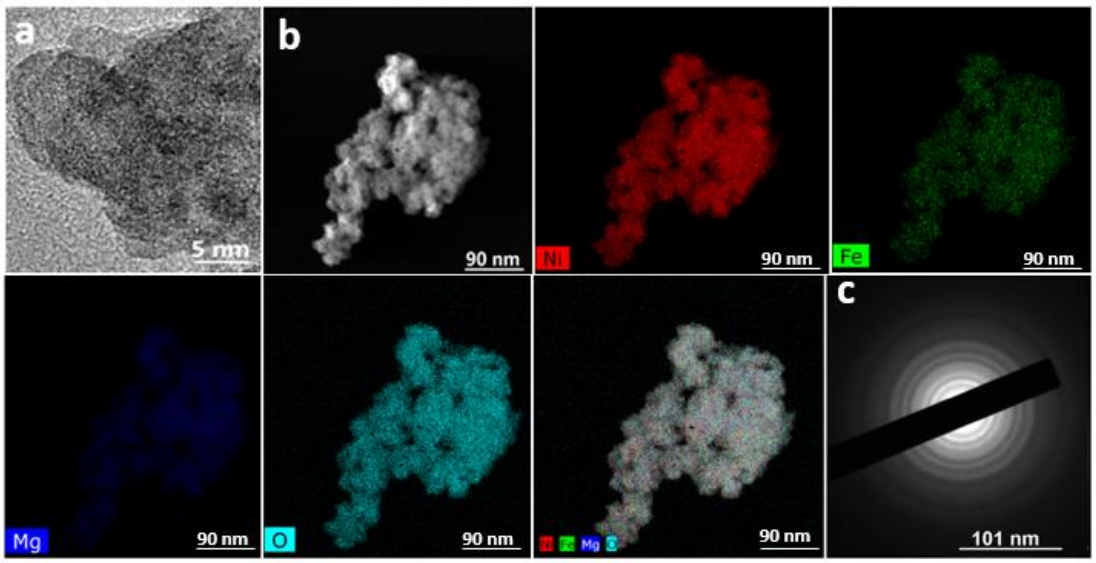

Figure S3 Morphology and composition characterization of Ni-Fe-Mg catalyst. Representative (a) TEM and (b) EDS elemental mapping of Ni-Fe-Mg catalyst, showing that the uniform, uncorrelated spatial distribution of Ni, Fe, and Mg; (c) selected area electron diffraction (SAED) analysis.

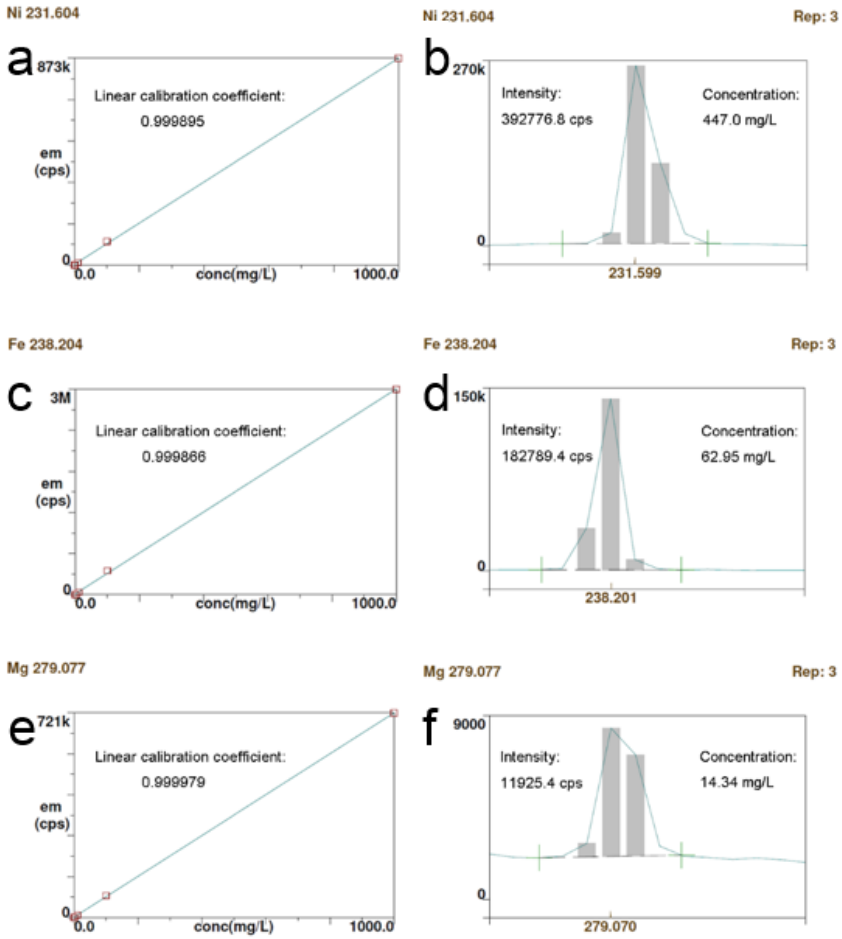

Figure S4 Calibration curve of inductively coupled plasma optical emission spectroscopy (ICP-OES) and ICP-OES spectra of Ni-Fe-Mg catalyst: Ni element (a, b), Fe element (c, d) and Mg element (e, f). The ratio of Ni:Fe:Mg is 7:1:0.2**.**

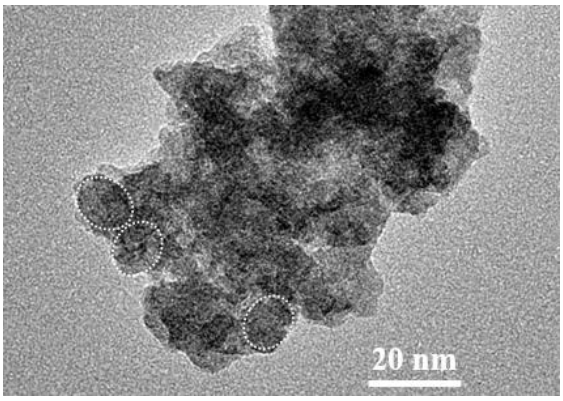

Figure S5 Surface TEM image of Ni-Fe-Mg catalyst. Ni-Fe-Mg catalyst mainly consisted of nanoparticles and presented porous morphology. The particle size is ~ 10 nm (showed in the dot line).

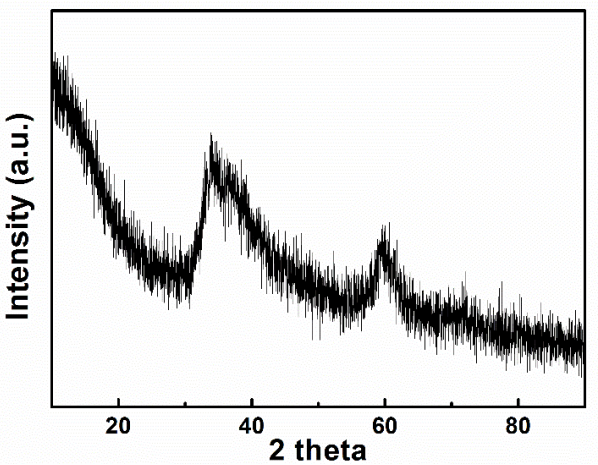

Figure S6 XRD of Ni-Fe-Mg catalyst. Ni-Fe-Mg catalyst revealed no evidence for a crystalline phase.

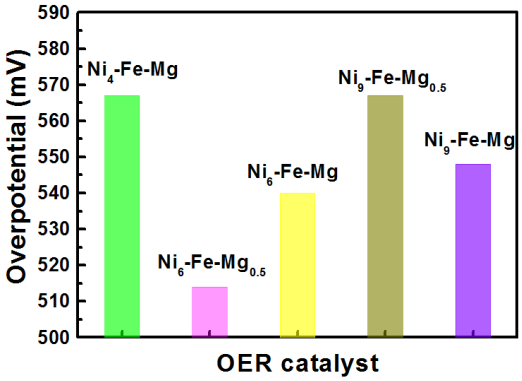

Figure S7 The overpotential change trend of different Ni/Fe/Mg ratios at 10 mA/cm^2 on GCE in CO_2-saturateed 0.5 M $KHCO_3$ electrolyte.

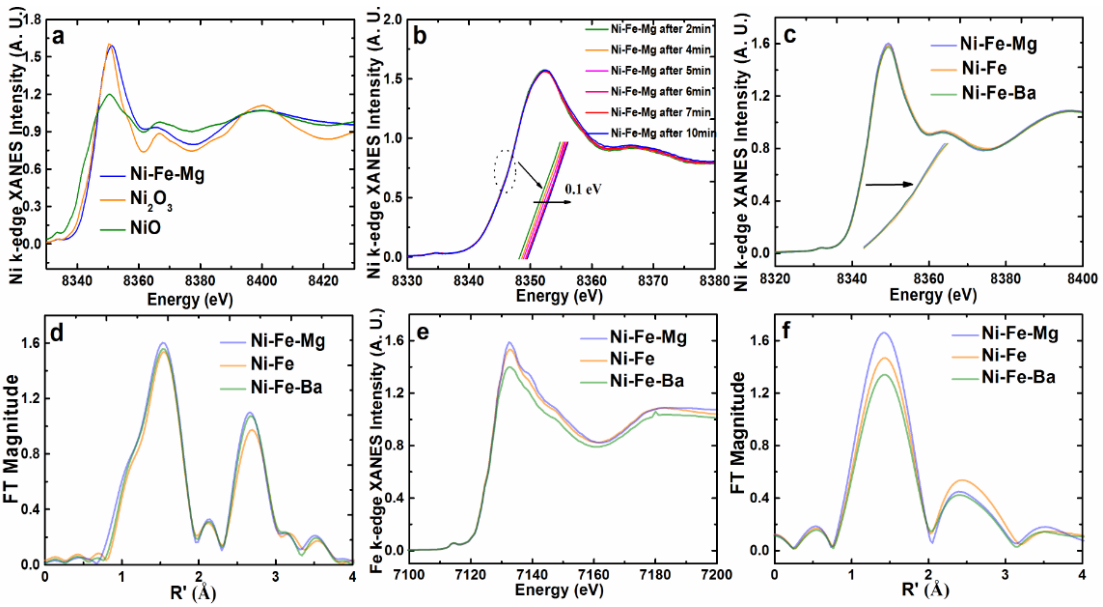

Figure S8 (a) The Ni K-edge XANES data of Ni-Fe-Mg catalyst, Ni_2O_3 and NiO controls after OER at 2.2 V (versus RHE). (b) The Ni K-edge XANES spectra after 2, 4, 5, 6, 7 and 10 min at 2.2 V (versus RHE). The Ni K-edge (c) XANES and (d) FT-EXAFS spectra of Ni-Fe, Ni-Fe-Mg and Ni-Fe-Ba catalysts after 15 min OER running at 2.2 V (versus RHE) in CO_2-saturated 0.5 M $KHCO_3$ aqueous electrolyte. The Fe K-edge (e) XANES and (f) FT-EXAFS spectra of Ni-Fe, Ni-Fe-Mg and Ni-Fe-Ba catalysts after 15 min OER running at 2.2 V (versus RHE) in CO_2-saturated 0.5 M $KHCO_3$ aqueous electrolyte.

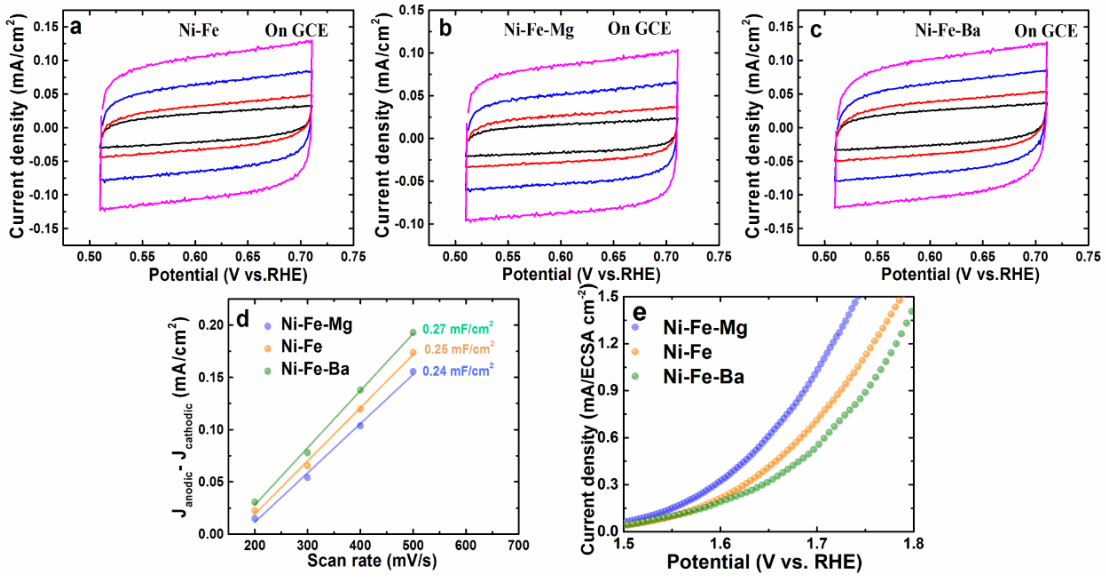

Figure S9 Cyclic voltammograms of (a) Ni-Fe, (b) Ni-Fe-Mg and (c) Ni-Fe-Ba catalysts in 0.8 - 1.0 V vs. RHE at scan rates from 200 to 500 mV/s in CO_2 saturated 0.5 M $KHCO_3$ aqueous electrolyte. (d) Scan rate dependence of the current densities of Ni-Fe, Ni-Fe-Mg and Ni-Fe-Ba and their corresponding linear fittings (solid lines). (e) LSV curves of three catalysts in three configurations in CO_2 saturated 0.5 M $KHCO_3$ aqueous electrolyte loaded on GCE and normalized by ECSA.

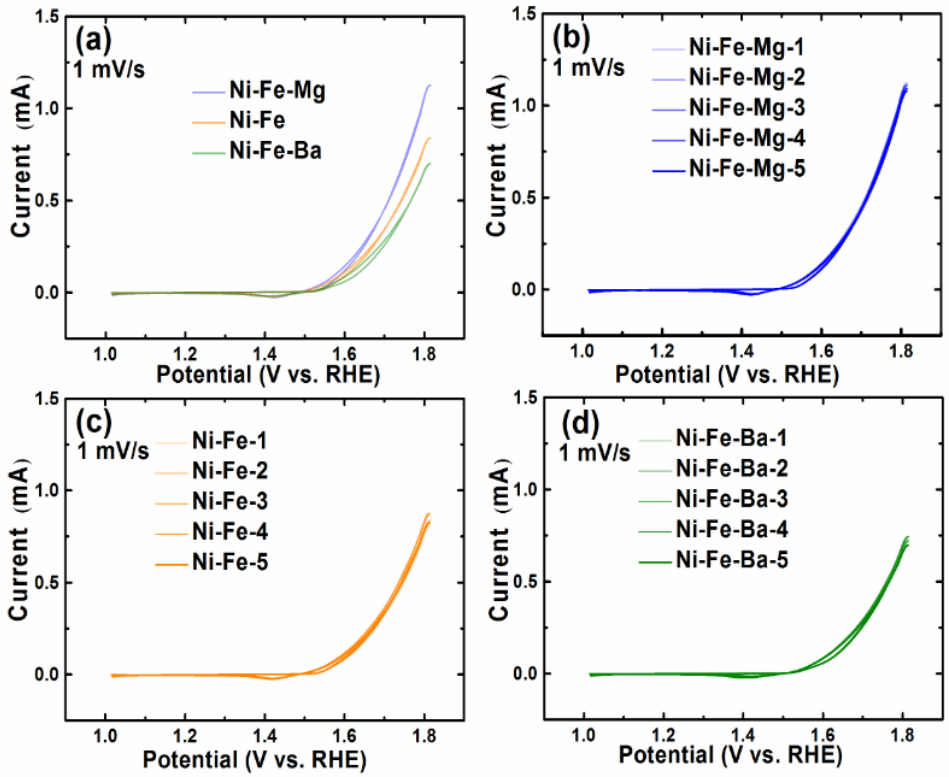

Figure S10 (a) Cyclic voltammograms of Ni-Fe, Ni-Fe-Mg and Ni-Fe-Ba catalysts at a scan rate of 1 mV/s in CO_2 saturated 0.5 M $KHCO_3$ aqueous electrolyte; five independent cyclic voltammograms curves of (b) Ni-Fe-Mg, (c) Ni-Fe and (d) Ni-Fe-Ba catalysts loaded on GCE with identical loading mass in three-electrode configuration in CO_2-saturated 0.5 M $KHCO_3$ aqueous electrolyte.

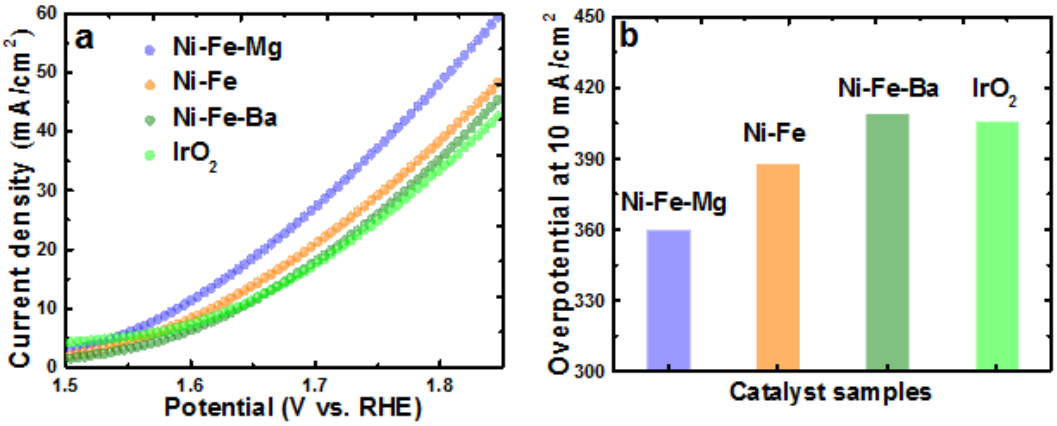

Figure S11 The (a) OER polarization curves and (b) overpotential of Ni-Fe-Mg catalysts and controls loaded on Ni foam in a three-electrode configuration in CO_2 saturated 0.5 M $KHCO_3$ aqueous electrolyte.

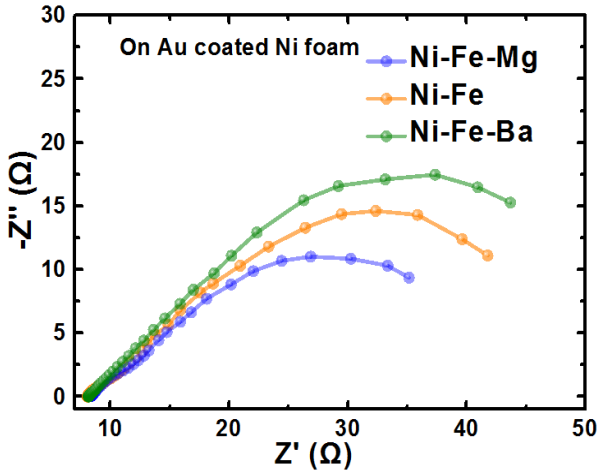

Figure S12 Electrochemical impedance spectroscopy (EIS) data for Ni-Fe-Mg catalysts and controls on Au coated Ni foam in three-electrode configuration in CO_2 saturated 0.5 M $KHCO_3$ aqueous electrolyte (The data were collected for the electrodes under 1.6 V vs. RHE).

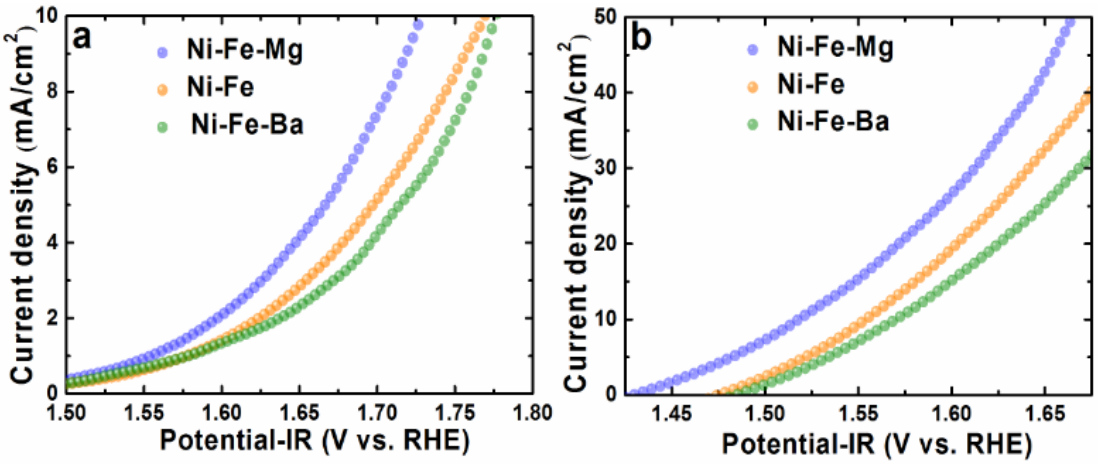

Figure S13 The OER polarization curves of Ni-Fe-Mg, Ni-Fe and Ni-Fe-Ba catalysts on (a) GCE and (b) Au coated Ni foam with identical loading mass after 95% iR correction (R is series resistance, obtained from EIS fitting).

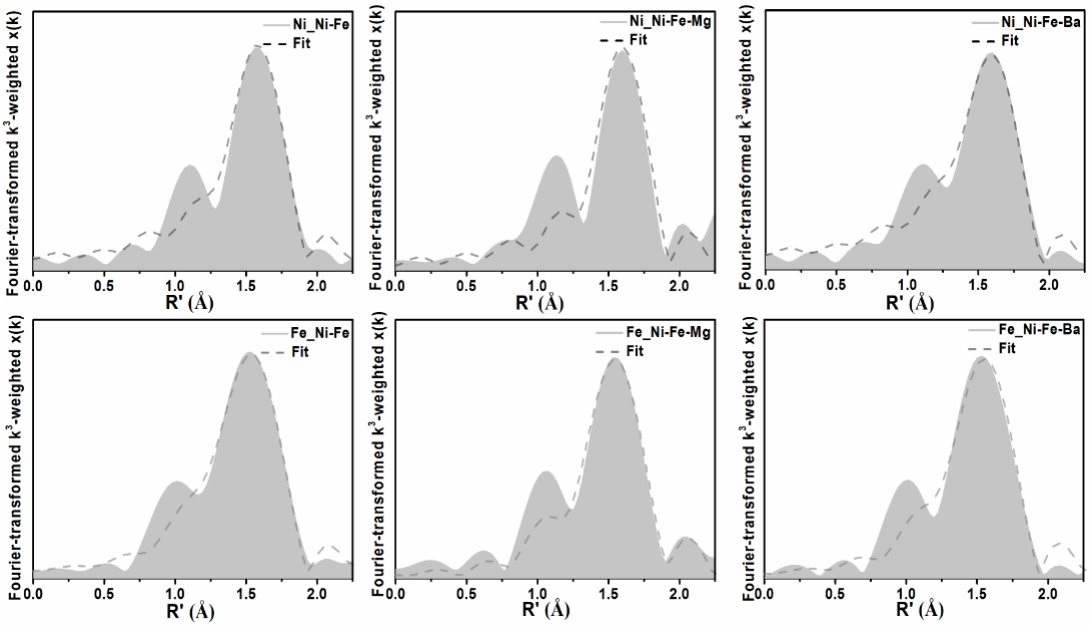

Figure S14 EXAFS spectra and fit of Ni and K-edge from Ni-Fe-Mg and the controls at open circuit and 2.2 V vs. RHE. The peak at 1.0–2.0 Å corresponds to the distance of Ni-O and Fe-O bond.

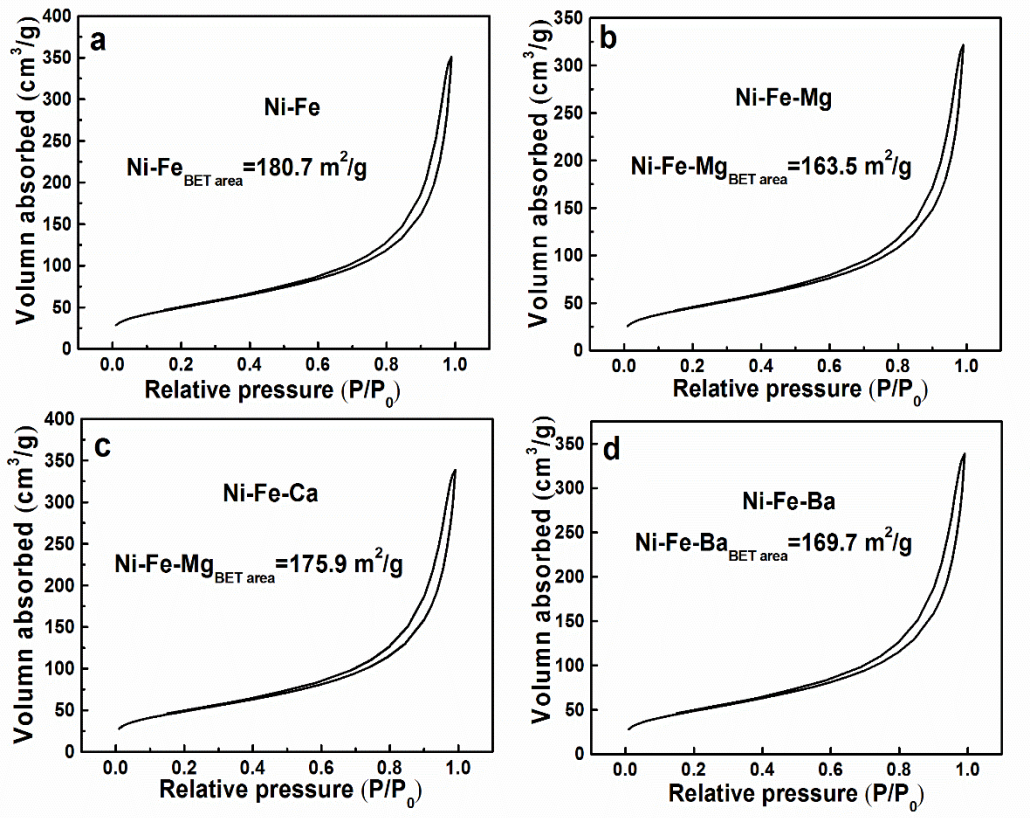

Figure S15 N_2 sorption isotherms of (a) Ni-Fe catalyst; (b) Ni-Fe-Mg catalyst; (c) Ni-Fe-Ca and (d) Ni-Fe-Ba catalyst.

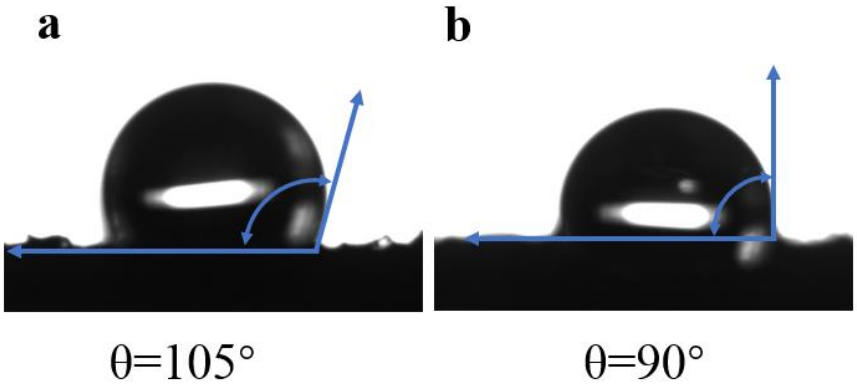

Figure S16 Contact angle measurement results of (a) Ni-Fe and Ni-Fe-Mg catalysts on carbon paper.

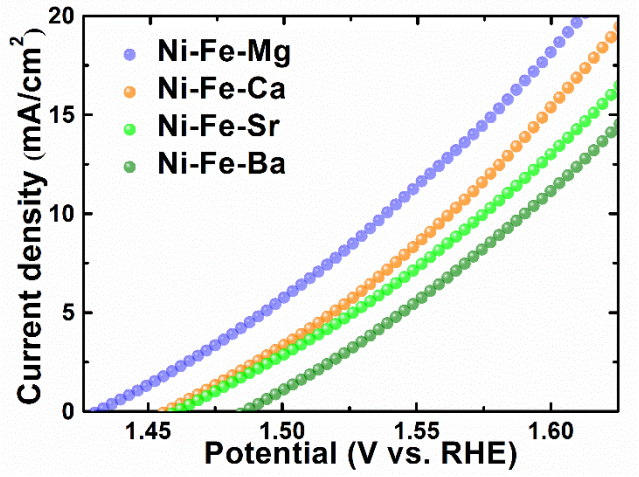

Figure S17 The (a) OER polarization curves and (b) overpotential of Ni-Fe-Mg catalysts and controls loaded on Au coated Ni foam in a three-electrode configuration in CO_2 saturated 0.5 M $KHCO_3$ aqueous electrolyte.

Table S1. Comparison of catalytic parameters of HEP Ni-Fe-Mg catalyst and controls.

Samples	pH	On GCE	On Ni Foam	On Au coated Ni Foam	References
		η at 10 mA/cm^2 (mV)	η at 10 mA/cm^2 (mV)	η at 10 mA/cm^2 (mV)	
Ni-Fe-Mg	**7.2**	**514**	**360**	**310**	**This work**
IrO_2	7.2	534	406	350	This work
Cu_6Co_7/CC	7.0	-	500[a]	-	J. Mater. Chem. A, 2018[11]
CoO/Co_4N	7.0	-	398	-	J. Mater. Chem. A, 2018[12]
NiFeCoP	7.2	560	-	330	Nat. Chem. 2018[13]
IrO_2	7.2	-	460[b]	-	Nat. Commun. 2015[14]
IrO_2	7.1	520[c]	-	-	Energy Environ. Sci. 2017[15]
Ni_3N@Ni-Ci	8.3	-	400[d]	-	J. Catal. 2017[16]
CoO/$CoSe_2$	8.3		510[d]	-	Adv. Sci. 2016[17]
$(Fe_xNi_{1-x})_2P$	7	-	396	-	Nano Energy[18]
Co_2P	7	592	-	-	Nano Let.2017[19]
Co-Pi	7	-	450[e]		Angew. Chem. Int. Ed. 2017[20]
Ni	7	-	600	-	Adv. Funct. Mater.2016[21]
NiFeCo	7	-	466	-	RSC Adv. 2016[22]
CoO	6.5	851	-	-	Nat. Commun. 2015[23]

a. Carbon cloth

b. Ti plate

c. FTO glass

d. on carbon paper at 20 mA/cm^2

e. Ti mesh

Table S2 Comparison of catalytic parameters of Ni-Fe, Ni-Fe-Mg and Ni-Fe-Ba catalysts.

Samples	Overpotential at 10 mA/cm^2 (mV)	Tafel slope (mV/dec)	TOF calculated by intergration of Ni redox	BET surface area (m^2/g)
Ni-Fe	565	170 ± 5	0.21	180.7
Ni-Fe-Mg	514	150 ± 3	0.30	163.5
Ni-Fe-Ba	568	210 ± 5	0.19	169.7

Table S3 Comparisons of ECSA and normalized current density (J_{ECSA}) at 1.7 V vs. RHE of Ni-Fe, Ni-Fe-Mg and Ni-Fe-Ba catalysts on different supports.

Samples	ECSA (cm^2)/ J_{ECSA} (mA per ECSA cm^{-2})	
	GCE	Au coated Ni foam
Ni-Fe-Mg	6.0/1.02	30.3/1.18
Ni-Fe	6.3/0.71	36.8/0.82
Ni-Fe-Ba	6.8/0.54	43.3/0.59

Table S4 Comparisons of TOF parameters of Ni-Fe, Ni-Fe-Mg and Ni-Fe-Ba catalysts on GCE at scan rate of 1 mV/s in CO_2 saturated 0.5 M $KHCO_3$ aqueous electrolyte.

Samples	Q (mC)	J (mA/cm^2)	TOF (/s)
Ni-Fe-Mg	0.98±0.03	8.49±0.2	0.30±0.02
Ni-Fe	0.97±0.07	6.41±0.4	0.23±0.03
Ni-Fe-Ba	0.97±0.07	5.13±0.2	0.19±0.02

Table S5 Comparisons of R_s of Ni-Fe, Ni-Fe-Mg and Ni-Fe-Ba catalysts on different supports.

Samples/Supports	R_s (Ω)	
	GCE	Au coated Ni foam
Ni-Fe-Mg	39.8	8.3
Ni-Fe	38.3	8
Ni-Fe-Ba	39.5	8.1

Table S6 Structural parameters from EXAFS data.

Samples	First shell	CN (Coordination number)	R (Å)(Bond distance)	σ^2 ($Å^{-2}$)	Edge
Ni-Fe	Ni-O	6.0±1.1	2.023±0.009	0.005±0.001	Ni K
	Fe-O	5.9±1.2	1.986±0.010	0.007±0.002	Fe K
Ni-Fe-Mg	Ni-O	6.0±0.5	2.020±0.008	0.003±0.001	Ni K
	Fe-O	5.6±1.3	1.960±0.012	0.003±0.002	Fe K
Ni-Fe-Ba	Ni-O	5.9±1.2	2.024±0.011	0.005±0.002	Ni K
	Fe-O	5.3±1.1	1.988±0.014	0.005±0.002	Fe K

Table S7 Comparisons of η at 10 mA/cm^2 for Ni-Fe-Mg, Ni-Fe and Ni-Fe-Ba on GCE in the electrolyte of different pH values.

	η at 10 mA/cm^2 on GCE (mV)		
Samples	Ni-Fe	Ni-Fe-Mg	Ni-Fe-Ba
pH~7	565	514	573
pH~8.5	500	470	494
pH~14	246	240	248

Table S8 Summary ICP-OES results of Ni-Fe-Mg and relevant controls.

Samples	Ni (ppm)	Fe (ppm)	Mg (ppm)	Ca (ppm)	Sr (ppm)	Ba (ppm)	Doping concentration ratio
Ni-Fe-Mg	427.276	63.593	19.913	-	-	-	4.6%
Ni-Fe-Ca	426.945	64.286	-	21.192	-	-	4.9%
Ni-Fe-Sr	442.232	74.174	-	-	26.882	-	6.0%
Ni-Fe-Ba	461.359	68.322	-	-	-	24.577	5.3%

References

[1] V. Fidelsky, M. C. Toroker, *Phys. Chem. Chem. Phys.* **2017**, *19*, 7491.

[2] M. Bajdich, M. GarcãA-Mota, A. Vojvodic, J. K. Nã¸Rskov, A. T. Bell, *J. Am. Chem. Soc.* **2013**, *135*, 13521.

[3] J.P. Perdew, K. Burke, M. Ernzerhof, *Phys. Rev. Lett.* **1996**, *77*, 3865.

[4] G. Kresse, *J. Non-Cryst. Solids* **1995**, *192-193*, 222.

[5] P.E. Blöchl, *Phys. Rev. B* **1994**, *50*, 17953.

[6] S. Grimme, J. Antony, S. Ehrlich, H. Krieg, *J. Chem. Phys.* **2010**, *132*, 154104.

[7] S. Nosé, *J. Chem. Phys.* **1984**, *81*, 511.

[8] M.J. Frisch, (Wallingford CT, **2009**).

[9] T.H.D. Jr, *J. Chem. Phys*. **1989**, *90*, 1007.

[10] P.J. Hay, *J. Chem. Phys*. **1985**, *82*, 299.

[11] M. Wang, W. Zhong, S. Zhang, R. Liu, J. Xing, G. Zhang, *J. Mater. Chem. A* **2018**, *6*, 9915.

[12] R.Q. Li, P. Hu, M. Miao, Y. Li, X.F. Jiang, Q. Wu, Z. Meng, Z. Hu, Y. Bando, X.-B. Wang, *J. Mater. Chem. A* **2018**, *6*, 24767.

[13] X. Zheng, B. Zhang, P. D. Luna, Y. Liang, R. Comin, O. Voznyy, L. Han, F. P. G. d. Arquer, M. Liu, C. T. Dinh. T. Regier, J. Dynes, S. He, H. L. Xin, H. S. Peng, D. Prendergast, X. W. Du, E. H. Sargent, *Nat. Chem.* **2018**, *10*, 149.

[14] M. Schreier, L. Curvat, F. Giordano, L. Steier, A. Abate, S. M. Zakeeruddin, J. Luo, M. T. Mayer, M. Grätzel, *Nat. Commun.* **2015**, *6*, 7326.

[15] Gurudayal, J. Bullock, D. F. Srankó, C. M. Towle, Y. Lum, M. Hettick, M. C.

Scott, A. Javey, J. Ager, *Energy Environ. Sci.* **2017**, *10*, 2222.

[16] F. Xie, H. Wu, J. Mou, D. Lin, C. Xu, C. Wu, X. Sun, *J. Catal.* **2017**, *356*, 165.

[17] K. Li, J. Zhang, R. Wu, Y. Yu, B. Zhang, *Adv. Sci.* **2016**, *3*, 1500426.

[18] B. Zhang, Y. H. Lui, H. Ni, S. Hu, *Nano Energy* **2017**, *38*, 553.

[19] K. Xu, C. Han, L. Liu, H. Lv, X. Wu, C. Wu, Y. Xie, *Nano Lett.* **2017**, *17*, 578.

[20]L. Xie, R. Zhang, L. Cui, D. Liu, S. Hao, Y. Ma, G. Du, A. M. Asiri, X. Sun, *Angew. Chem. Int. Ed.* **2017**, *56*, 1064.

[21] H. Schäfer, D. M. Chevrier, P. Zhang, J. Stangl, K. Müller-Buschbaum, J. D. Hardege, K. Küpper, J. Wollschläger, U. Krupp, S. Dühnen, *Adv. Funct. Mater.* **2017**. *26*, 6402.

[22] Z. Zhang, J. Hao, W. Yang, J. Tang, *RSC Adv.* **2016**, *6*, 9647.

[23] C. W. Tung, Y. Y. Hsu, Y. P. Shen, Y. Zheng, T. S. Chan, H. S. Sheu, Y. C. Cheng, H. M. Chen, *Nat. Commun.* **2015**, *6*, 8106.